Mon. Not. R. Astron. Soc. **000**, 000–000 (0000) Printed 9 August 2016 (MN LATEX style file v2.2)

The underlying driver for the C IV Baldwin effect in QSOs with $0 < z < 5$

Xue Ge, Wei-Hao Bian ⋆, Xiao-Lei Jiang, Wen-Shuai Liu and Xiao-Feng Wang
Department of Physics and Institute of Theoretical Physics, Nanjing Normal University, Nanjing 210023, China

arXiv:1608.02172v1 [astro-ph.GA] 7 Aug 2016

9 August 2016

ABSTRACT

Broad emission lines is a prominent property of type I quasi-stellar objects (QSOs). The origin of the Baldwin effect for C IV $\lambda1549$ Å broad emission lines, i.e., the luminosity dependence of the C IV equivalent width (EW), is not clearly established. Using a sample of 87 low-z Palomar-Green (PG) QSOs and 126 high-z QSOs across the widest possible ranges of redshift ($0 < z < 5$), we consistently calculate Hβ -based single-epoch supermassive black hole (SMBH) mass and the Eddington ratio to investigate the underlying driver of the C IV Baldwin effect. An empirical formula to estimate the host fraction in the continuum luminosity at 5100 Å is presented and used in Hβ -based $M_{\rm BH}$ calculation for low-z PG QSOs. It is found that, for low-z PG QSOs, the Eddington ratio has strong correlations with PC1 and PC2 from the principal component analysis, and C IV EW has a strong correlation with the optical Fe II strength or PC1. Expanding the luminosity range with high-z QSOs, it is found that C IV Baldwin effect exists in our QSOs sample. Using Hβ -based single-epoch SMBH mass for our QSOs sample, it is found that C IV EW has a strong correlation with the Eddington ratio, which is stronger than that with the SMBH mass. It implies that the Eddington ratio seems to be a better underlying parameter than the SMBH mass to drive the C IV Baldwin effect.

Key words: black hole physics — galaxies:active — quasars:emission lines

1 INTRODUCTION

Broad emission lines is a prominent property of type I active galactic nuclei (AGNs) and quasi-stellar objects (QSOs). It is accepted that these broad emission lines are produced by photoionization in broad-line regions (BLRs) gas, where the accretion disc surround the central supermassive black hole (SMBH) provides the ionizing photos. Baldwin (1977) discovered an anti-correlation between the equivalent width (EW) of the C IV $\lambda1549$ Å emission line and the continuum luminosity in the QSO rest frame, (i.e. the Baldwin effect, see the review by Shields 2007). Over the past 20 yr, this effect was investigated with different QSOs samples, including other permitted/prohibited emission lines, such as Lyα, C III , Si IV , Mg II , [O III] , Fe Kα (e.g., Green et al. 2001; Dietrich et al. 2002; Shang et al. 2003; Baskin & Laor 2004; Xu et al. 2008; Wu et al. 2009; Richards et al. 2011; Bian et al. 2012; Shen & Ho 2014).

It is believed that the Baldwin effect exists for many UV/optical emission lines. However, its origin is not clearly established. One promising interpretation is the softening of the spectral energy distribution (SED) for increasing luminosity, which lowers the ion populations that having high ionization potentials (e.g., Netzer et al. 1992; Dietrich et al. 2002). Non-isotropic continuum emission and the intrinsic Baldwin effect would provide some of the observed scatter in the Baldwin effect (e.g., Baskin & Laor 2004). The underlying physical parameters for the Baldwin effect are investigated for many years, such as the eigenvector 1 of Boroson & Green (1992), the Eddington ratio $L_{\rm Bol}/L_{\rm Edd}$ (i.e. the ratio of the bolometric luminosity to the Eddington luminosity), the SMBH mass $M_{\rm BH}$ (e.g., Boroson & Green 1992; Wills et al. 1999; Boroson 2002; Shang et al. 2003; Bachev et al. 2004; Baskin & Laor 2004; Xu et al. 2008; Bian et al. 2012; Shemmer & Lieber 2015). For a optical-selected sample of Palomar-Green (PG) QSOs, Baskin & Laor (2004) found a strong correlation of the C IV EW with $L_{\rm Bol}/L_{\rm Edd}$, stronger than that with the continuum luminosity, and suggested that the $L_{\rm Bol}/L_{\rm Edd}$ is the primary physical parameter which drives the C IV Baldwin effect (Shemmer & Lieber 2015). Using a larger sample of QSOs with $1.5 < z < 5$ from Sloan Digital Sky Survey (SDSS), Xu et al. (2008) found the C IV EW has a stronger correlation with C IV-based $M_{\rm BH}$ than the $L_{\rm Bol}/L_{\rm Edd}$. Using C IV-based $M_{\rm BH}$ by Shen et al. (2011) for high-z SDSS QSOs, Bian et al. (2012) also found that there is a correlation between the C IV EW and the C IV -based $M_{\rm BH}$. However, with Mg II-based $M_{\rm BH}$, Bian et al. (2012) found SDSS QSOs in $1.5 < z < 1.9$ follow the relation found by Baskin & Laor (2004), suggesting the bias in C IV-based $M_{\rm BH}$.

Due to the larger consumption of telescope time in reverberation mapping (RM), there is about 60 AGN/QSOs with reliable BLRs sizes from RM (Kaspi et al. 2000; Peterson et al. 2004;

⋆ E-mail: whbian@njnu.edu.cn

© 0000 RAS

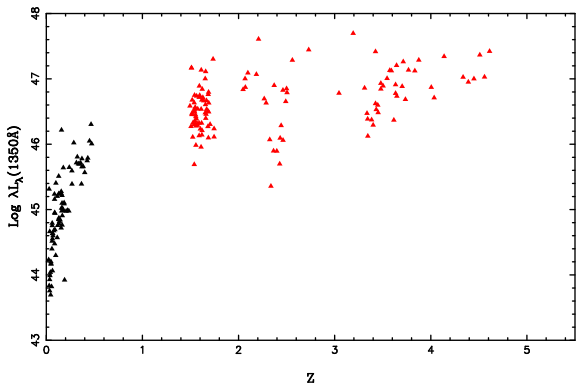

Figure 1. The UV continuous luminosity at 1350Å (in units of erg/s) versus redshift for our low-z and high-z sample. The black triangles denote 87 low-z PG QSOs, and the red triangles denote 126 high-z QSOs.

Du et al. 2016; Shen et al. 2016). From the RM BLRs sizes, there is an empirical R-L relation (Kaspi et al. 2000; Bentz et al. 2013; Du et al. 2015). With this empirical R-L relation, the BLRs size can be derived from the continuum luminosity at 5100 Å. The single-epoch SMBH mass can be calculated from the broad emission lines, such as Hβ , Hα , Mg II , C IV (e.g., Laor 1998; Bian & Zhao 2004; Greene & Ho 2005; Vestergaard & Peterson 2006; Jun et al. 2015). By the host correction in the continuum luminosity at 5100 Å by Hubble Space Telescope (HST) images for different width slits, Bentz et al. (2013) found that the slope in R-L relation changes from 0.7 to 0.533. It is suggested that C IV -based $M_{\rm BH}$ is biased to the Hβ -based $M_{\rm BH}$ (e.g., Rafiee & Hall 2011; Shen & Liu 2012; Bian et al. 2012). For high-z QSOs, the Hβ emission line is shifted to the infrared (IR) band. The IR spectroscopy observation for high-z QSOs is needed to calculate SMBH $M_{\rm BH}$ using the same Hβ emission line as that for low-z QSOs.

In order to investigate the C IV EW relation with the SMBH accretion, we compile a sample of 87 low-z PG QSOs and 126 high-z QSOs across the widest possible ranges of redshift ($0 < z < 5$) with available spectral information for Hβ λ4861 Å and C IV λ1549 Å emission lines. Our adopted sample is described in §2, the results and the analysis are given in §3, and the conclusions are presented in §4. All of the cosmological calculations in this paper assume $H_0 = 70$ km s^{-1} Mpc^{-1}, $\Omega_M = 0.3$, and $\Omega_\Lambda = 0.7$.

2 SAMPLE

2.1 low-z sample

The 87 PG QSOs ($0 < z < 0.5$) are optically selected by a limiting B-band magnitude of 16.16, blue $U - B$ colour (< -0.44), and dominant starlike appearance, showing broad emission lines classified as type 1 QSOs (Schmidt & Green 1983; Boroson & Green 1992). The low-z PG QSOs is representative of bright optically selected QSOs (Jester et al. 2005). It is the most thoroughly explored sample of AGN/QSOs, with a lot of high quality data at most wave bands (e.g., Boroson & Green 1992; Brandt et al. 2000; Baskin & Laor 2004; Bian et al. 2014; Shi et al. 2014). Boroson & Green (1992) observed all these 87 PG QSOs with the KPNO 2.1 m telescope and the Gold Spectrograph. The spectra of these objects were made through a 1.5 arcsec slit with a spectral resolution of about 6.5 Å, covering the range 4300-5700 Å in the rest frame. In this paper, the Hβ width at half-maximum (FWHM) is adopted from Boroson & Green (1992) used in the Hβ -based single epoch SMBH mass calculation (see also Boroson 2002; Vestergaard & Peterson 2006). In Table 1, the spectral-resolution-corrected Hβ FWHM adopted from Vestergaard & Peterson (2006) is listed in Col. (9). For UV spectra of these 87 PG QSOs, Baskin & Laor (2004) obtained archived UV spectra for these 85 PG QSOs, 47 from the HST and 38 from the International Ultraviolet Explorer (IUE). For three of them (PG 0934+013, PG 1004+130, PG 1448+273), their UV archival spectra did not have a sufficient S/N to measure the C IV EW, and PG 1700+518 is a broad-absorption line (BAL) QSOs. In addition, there are five BAL QSOs and 16 radio-loud (RL) QSOs. The continuum luminosity at 1350 Å / 5100 Å is calculated from the (SED) presented by Neugebauer et al. (1987) (Baskin & Laor 2004; Vestergaard & Peterson 2006). Table 1 lists the information of 87 PG QSOs. Fig. 1 shows $\lambda L_\lambda(1350\AA)$ versus z, where black triangles denote 87 PG QSOs.

2.2 High-z sample

In this paper, the Hβ emission line is needed to calculate the single-epoch $M_{\rm BH}$ for all QSOs and to investigate the underlying parameter for the C IV Baldwin effect. For high-z QSOs with available C IV λ1459 Å observed by ground telescope ($z > 1.5$), the Hβ emission line is shifted to the IR band.

Shen & Liu (2012) presented 60 intermediate-redshift QSOs ($z \sim 1.5 - 2.2$) selected from SDSS DR7. Their near-IR spectrum are observed with TripleSpec (Wilson et al. 2004) ($0.95 - 2.46\ \mu m$) on the ARC 3.5 m telescope, and with the Folded-port InfraRed Echellette (Simcoe et al. 2010) ($0.8 - 2.5\ \mu m$) on the 6.5 m Magellan-Baade telescope. With TripleSpec, the total exposure is typically $1 - 1.5$ hr with slits widths of both 1.1″ and 1.5″, and the resulting spectral resolution of $R \sim 2500 - 3500$. With FIRE, typical total exposure times were 45 min with the slit width of 0.6″. The spectral resolution is $R \sim 6000$ (50 km s^{-1}). They performed standard ABBA dither patterns to aid sky subtraction and observed a nearby A0V star as flux and telluric standard. Jun et al. (2015) presented near-Infrared grism spectra for 155 QSOs ($3.3 < z < 6.4$) from the $AKARI$ space telescope. It is composed of optically luminous and spectroscopically confirmed type 1 QSOs at $z > 3$, mostly out of SDSS DR5. The spectrum coverage is $2.5 - 5.0\ \mu m$. The spectral resolution is $R = 120$ at $3.6\mu m$, corresponding to a velocity resolution of 2500 km s^{-1} . Jun et al. (2015) gave 43 high-z QSOs with Hα information. From above two literatures and others (Shemmer et al. 2004; Netzer et al. 2007; Dietrich et al. 2009; Assef et la. 2011; Ho et al. 2012; Shen & Liu 2012; Jun et al. 2015; Shemmer & Lieber 2015), we assembled a sample of 182 high-z QSOs with Hβ /Hα data.

In order to obtain the UV C IV data for these high-z QSOs, we search their SDSS spectral data. The SDSS used a 2.5-m wide-field telescope at Apache Point Observatory near Sacramento Peak in Southern New Mexico to conduct an imaging and spectroscopic survey. Shen et al. (2011) presented a compilation of properties of the 105,783 QSOs in the SDSS DR7 catalogue, where they used multi-Gaussians to fit the main emission lines, such as C IV , Mg II , Hβ , Hα depending on the redshift. We search these 182 high-z QSOs in the SDSS DR7 QSOs sample by Shen et al. (2011), and obtain 126 high-z QSOs with C IV fitting data and the luminosity at 1350 Å. Shen et al. (2011) suggested that measurements of C IV EW for most objects are unbiased to within 20% down to S/N $\sim$ 3. For our SDSS high-z sample, their S/N are larger than 3. There are 7 BAL QSOs, 12 RL QSOs, 11 weak line QSOs

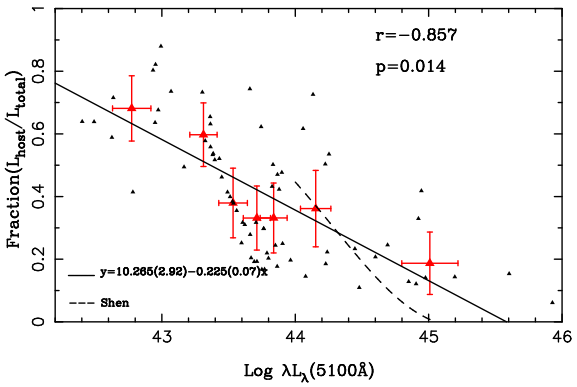

Figure 2. The host fraction in the total continuum luminosity at 5100 Å versus the total continuum luminosity at 5100 Å. The black triangles are the observation data from (Bentz et al. 2013), the red triangle denotes the value of each bin. The black solid line is the best fit for bin data. The dotted line is the formula from (Shen et al. 2011). For red bin data, the Spearman correlation coefficient and the probability of the null hypothesis are shown in the panel.

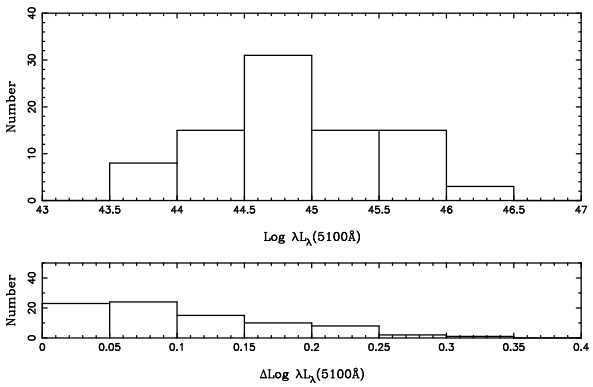

Figure 3. Top: distribution of total continuum luminosity at 5100 Å. Bottom: distribution of the difference between the total continuum luminosity and the nuclei continuum luminosity at 5100 Å in logarithm, i.e., $log(1/(1-f))$.

(EW(CIV) < 10Å). For these 126 high-z QSOs, we respectively select 10, 15, 7, 1, 60, 7, and 26 high-z QSOs from the literatures of Shemmer et al. (2004); Netzer et al. (2007); Assef et la. (2011); Ho et al. (2012); Shen & Liu (2012); Shemmer & Lieber (2015); Jun et al. (2015). For 26 high-z QSOs in Jun et al. (2015), we obtain the $\lambda L_\lambda(5100\AA)$ and Hα FWHM from table 7 in Jun et al. (2015). We convert the Hα FWHM to Hβ FWHM by the formula (Jun et al. 2015),

$$\log \frac{\mathrm{FWHM(H}\beta)}{1000\ \mathrm{km\ s^{-1}}}) = (1.061 \pm 0.013)\log \frac{\mathrm{FWHM(H}\alpha)}{1000\ \mathrm{km\ s^{-1}}} + (0.055 \pm 0.008). \quad (1)$$

The FWHM of Hα or Hβ is listed in Col. (7) in Table 2. These 126 high-z QSOs are used as our final high-z QSOs sample with available Hβ and C IV data at the same time. It is larger than the high-z sample of 36 QSOs ($z < 3.5$) by Shemmer & Lieber (2015). Our sample covers the redshift of $0 < z < 5$ and the $log\lambda L_\lambda(1350\AA)$ of $43.6-47.7$. Table 2 lists the properties of high-z QSOs. In Fig. 1, the red triangles denote these 126 high-z QSOs.

3 RESULT AND DISCUSSION

3.1 The host contribution in the continuum luminosity at 5100 Å

With the empirical R-L relation, the BLRs size can be derived from the nuclei continuum luminosity. Based on the stacked SDSS spectra, Shen et al. (2011) gave an empirical formula to give the ratio of host to nuclei QSOs luminosity for the total QSOs continuum luminosity of $log(\lambda L_\lambda(5100\AA)/erg\ s^{-1}) = 44.1 - 45.5$. When total QSOs luminosity are larger than $10^{45} erg/s$, the host contribution is negligible. For high-z QSOs in our sample, we found they are all $log(\lambda L_\lambda(5100\AA)/erg\ s^{-1}) > 45$, and the host contamination is generally negligible. For low-z PG QSOs, we need to correct the host contribution to derive the BLRs sizes because of their lower luminosity at 5100Å.

Using GALFIT (Peng et al. 2002) to model HST host-galaxy images of 41 RM AGN Bentz et al. (2013) did the host correction for 71 observation data at 5100 Å. For the host fraction in the total continuum luminosity from (Bentz et al. 2013), we bin the observation data into seven bins according the total continuum luminosity at 5100 Å. The value of each bin is the average of total continuum luminosity and the host fraction, and the error of each bin value is the standard deviation. For the bin data, the Spearman correlation test gives the Spearman correlation coefficient $r_s = 0.86$ and the probability of the null hypothesis $P_{\rm null} = 1.4\times10^{-2}$. The relationship is derived by using algorithms FITEXY (Press et al. 1992).

$$f = (10.265 \pm 2.92) - (0.225 \pm 0.07)\ log\lambda L_\lambda(5100\AA)^{total} \quad (2)$$

where f is the host fraction in the total continuum luminosity at 5100 Å, $\lambda L_\lambda(5100\AA)^{total}$ is the total continuum luminosity at 5100 Å. In Fig. 2, we also show the host fraction formula of Shen et al. (2011) for SDSS fibre, which is consistent with our formula, considering the decreasing tendency with large $\lambda L_\lambda(5100\AA)$. The host fraction decreases from about 80% at $\lambda L_\lambda(5100\AA) = 10^{42} erg/s$ to about 10% at $\lambda L_\lambda(5100\AA) = 10^{45} erg/s$.

For 87 low-z PG QSOs, there are 16 RM objects, where the host fractions are adopted from Bentz et al. (2013). For other PG QSOs with the total continuum luminosity $\lambda L_\lambda(5100\AA)$ below $10^{45.5} erg/s$, we use our formula to correct the host contribution. The host-corrected $\lambda L_\lambda(5100\AA)$ is listed in Col. (8) in Table 1. Fig. 3 shows the distribution of total luminosity at 5100 Å (top panel) for 87 PG QSOs and the distribution of the difference between the total continuum luminosity and the nuclei continuum luminosity at 5100 Å in logarithm, i.e., $log(1/(1-f))$ (bottom panel). Considering the range of log $\lambda L_\lambda(5100\AA)$ of $43.6 - 46.2$, the host fraction f in the total luminosity at 5100Å is estimated to be less than about 50% from our formula of Eq. 2. $log(1/(1-f)) = 0.3$ for $f = 50\%$ (bottom panel in Fig. 3).

3.2 $M_{\rm BH}$ and $L_{\rm Bol}/L_{\rm Edd}$

Using 32 RM SMBHs masses from Peterson et al. (2004), Vestergaard & Peterson (2006) gave a formula to calculate the SMBH mass from the AGN/QSOs single-epoch spectrum, where Hβ FWHM and the continuum luminosity at 5100 Å are measured.

$$logM_{\rm BH}(H\beta) = log\{(\frac{\mathrm{FWHM(H}\beta)}{1000\ \mathrm{km\ s^{-1}}})^2 \times (\frac{\mathrm{\lambda L_\lambda(5100\AA)}}{10^{44}\ \mathrm{erg\ s^{-1}}})^{0.5}\} + (6.91 \pm 0.02) \quad (3)$$

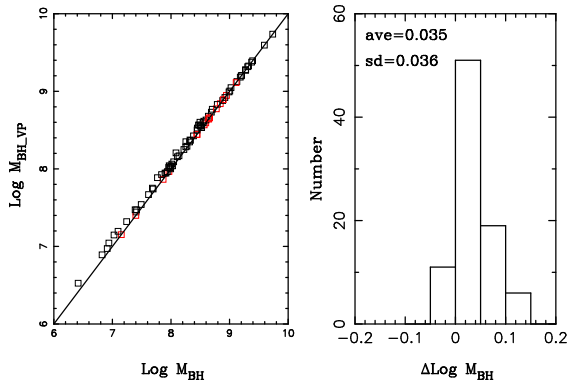

Figure 4. Left: $M_{\rm BH}$ given in (Vestergaard & Peterson 2006) versus our calculated $M_{\rm BH}$ considering host contribution for 87 low-z PG QSOs. The red square denotes 16 RM objects. The black line is 1:1. Right: distribution of the $M_{\rm BH}$ difference.

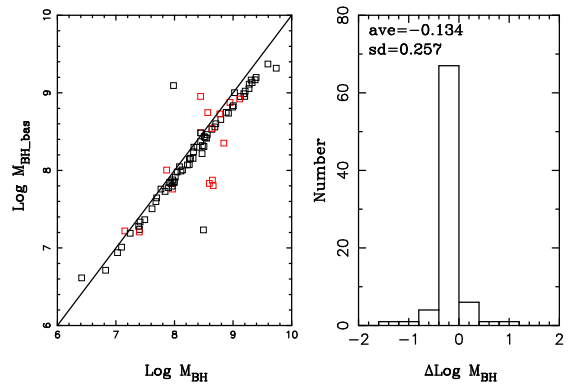

Figure 5. Left: $M_{\rm BH}$ given in (Baskin & Laor 2004) versus our calculated $M_{\rm BH}$ considering host contribution for 87 low-z PG QSOs. The red square denotes 16 RM objects. The black line is 1:1. Right: distribution of the $M_{\rm BH}$ difference.

With above formula, we calculate the black hole mass using FWHM(Hβ) and host-corrected continuum luminosity at 5100 Å for 71 non-RM low-z PG QSOs and 126 high-z QSOs (see Tables 1 and 2). The host-corrected $M_{\rm BH}$ is listed in Col. (10) in Table 1 for low-z PG QSOs. We also list the $M_{\rm BH}$ given by Vestergaard & Peterson (2006) in Col. (11) and that by Baskin & Laor (2004) in Col. (12) in Table 1. Fig. 4 shows $M_{\rm BH}$ given in Vestergaard & Peterson (2006) (without host correction, same formula) versus our calculated $M_{\rm BH}$ considering host correction for 87 low-z PG QSOs (left-hand panel) and the distribution of their $M_{\rm BH}$ difference (right-band panel). The red squares denote RM objects. The mean value of their difference is 0.035 with the standard deviation of 0.036. Considering that $M_{\rm BH} \propto L^{0.5}$, the $\log\lambda L_\lambda(5100\AA)$ correction of 0.1 dex would lead to a decrease of 0.05 dex, which is consistent with the result in Fig. 4. With a different formula by Laor (1998), Baskin & Laor (2004) also calculated the $M_{\rm BH}$ for 87 PG QSOs. Fig. 5 shows our calculated $M_{\rm BH}$ versus that in Baskin & Laor (2004) (left-hand panel) and the distribution of their difference (right-hand panel). The mean value of their difference is 0.134 dex with the standard deviation of 0.257. Considering intrinsic scatter in $M_{\rm BH}$ calculation of about 0.3 dex (e.g., Shen et al. 2011), the host correction in $M_{\rm BH}$ calculation is negligible for low-z PG QSOs sample, although it is important for low-

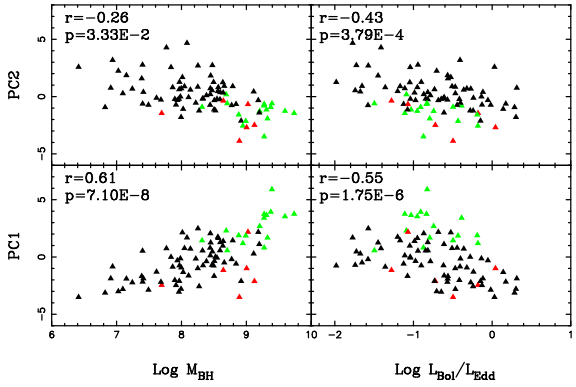

Figure 6. Left: the relationship between $M_{\rm BH}$ and PC1, PC2. Right: the relationship between Eddington ratio $L_{\rm Bol}/L_{\rm Edd}$ and PC1, PC2. Green triangles denote RL QSOs. Red triangles denote BAL QSOs. The Spearman correlation coefficient and the probability of the null hypothesis is shown in the left in each panel.

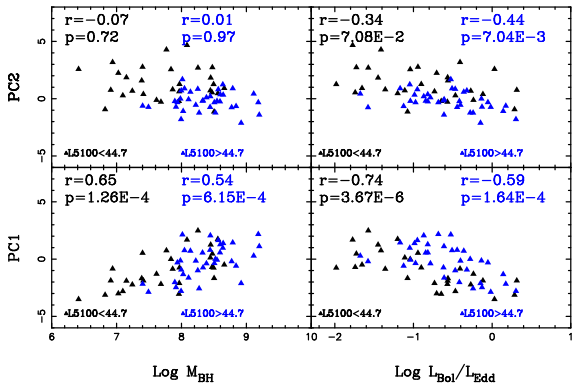

Figure 7. The same as Fig. 6 but for two subsamples dividing by luminosity $log\lambda L_\lambda(5100\AA) = 44.7$ (excluding RL QSOs and BAL QSOs). The back triangles denote PG QSOs with smaller $\lambda L_\lambda(5100\AA)$ and blue triangles denote PG QSOs with larger $\lambda L_\lambda(5100\AA)$. The Spearman correlation coefficient and the probability of the null hypothesis is shown in each panel.

luminosity AGN/QSOs. For high-z QSos, the $M_{\rm BH}$ is also listed in Col. (9) in Table 2.

We use the nuclei continuum luminosity at 5100Å to calculate the bolometric luminosity by a bolometric correction of 9.26 (Richards et al. 2006), and then calculate the Eddington ratio $L_{\rm Bol}/L_{\rm Edd}$ for our low-z QSOs. For high-z QSOs, $\lambda L_\lambda(5100\AA)$ is so large that the host contribution can be neglected, and $L_{\rm Bol}/L_{\rm Edd}$ are calculated as that for low-z PG QSOs. $L_{\rm Bol}/L_{\rm Edd}$ for high-z QSOs is listed in Col. (10) in Table 2.

3.3 The relation between the SMBH accretion and PC1/PC2 from PCA

With the optical spectral information and additional information from other bands for 87 low-z PG QSOs, Boroson & Green (1992) presented principal component analysis (PCA) and found that the variance in the optical emission lines and the continuum (radio through X-ray) was mostly contained in two sets of correlations, eigenvectors of the correlation matrix. Principal component 1 (PC1) links the strength of optical Fe II emission, [O III] emission, and Hβ line asymmetry. Principal component 2 (PC2) in-

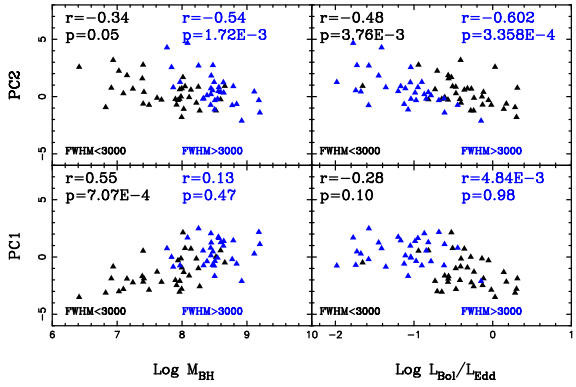

Figure 8. Same as Fig. 6 but for two subsamples dividing by $FWHM(H\beta) = 3000\mathrm{km\,s^{-1}}$ (excluding RL QSOs and BAL QSOs). The back triangles denote PG QSOs with smaller Hβ FWHM and blue triangles denote PG QSOs with larger Hβ FWHM. The Spearman correlation coefficient and the probability of the null hypothesis is shown in each panel.

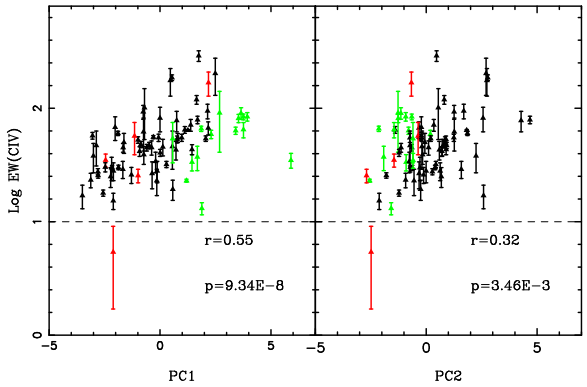

Figure 9. Left: the relationship between C IV EW and PC1. Right: the relationship between C IV EW and PC2. The marks are the same as Fig. 6

volves optical luminosity and the strength of He II 4686 and $\alpha_{\rm ox}$. With the single-epoch SMBH mass derived from Hβ (Kaspi et al. 2000), Boroson (2002) found that PC1 is mainly correlation with $L_{\rm Bol}/L_{\rm Edd}$ and PC2 has a strong correlations with $M_{\rm BH}$ and $L_{\rm Bol}/L_{\rm Edd}$. He suggested that PC1 is driven predominantly by the Eddington ratio, and PC2 is driven by the accretion rate. The coefficient listed in table 1 in Boroson (2002) is used to calculate the PC1/PC2 values. PC1/PC2 values are listed in Col. (15-16) in Table 1. Fig. 6 shows PC1/PC2 versus our calculated $M_{\rm BH}$ and $L_{\rm Bol}/L_{\rm Edd}$ for 87 low-z PG QSOs. We find that PC1 has strong correlations with $M_{\rm BH}$ and $L_{\rm Bol}/L_{\rm Edd}$, r=0.66, -0.46, respectively. PC2 has a strong correlation with $M_{\rm BH}$ and a weak correlation with $L_{\rm Bol}/L_{\rm Edd}$, r=-0.53, -0.34, respectively. These results are consistent with Boroson (2002). In Fig. 6, we also show 16 RL QSOs (green triangle) and 5 BAL QSOs (red triangle). Considering the speciality RL QSOs and BAL QSOs, we exclude them and find that PC1 still has strong correlation with $M_{\rm BH}$ and $L_{\rm Bol}/L_{\rm Edd}$, r=0.61, -0.55, respectively. PC2 has a weak correlation with $M_{\rm BH}$ and a strong correlation with $L_{\rm Bol}/L_{\rm Edd}$, r=-0.26, -0.43, respectively. It is different to the results by Boroson (2002), where PC2 has a very weak correlation with $L_{\rm Bol}/L_{\rm Edd}$ and a strong correlation with $M_{\rm BH}$. With our calculated $M_{\rm BH}$ and $L_{\rm Bol}/L_{\rm Edd}$ and excluding RL QSO ang BAL QSO, we find that PC2 has a strong correlation with $L_{\rm Bol}/L_{\rm Edd}$ and a weak correlation with $M_{\rm BH}$. We think it is due to narrower PC1/PC2 parameter space (see Fig. 6).

In Fig. 7, we divide low-z PG QSOs into two parts at $log\lambda L_{\lambda}(5100\mathring{A}) = 44.7$. For low-luminosity part, PC1 has strong correlations with $M_{\rm BH}$ and $L_{\rm Bol}/L_{\rm Edd}$. PC2 has weak correlations with $M_{\rm BH}$ and $L_{\rm Bol}/L_{\rm Edd}$. For high-luminosity part, PC1 still has strong correlations with $M_{\rm BH}$ and $L_{\rm Bol}/L_{\rm Edd}$. PC2 has a weak correlation with $M_{\rm BH}$ and a strong correlation with $L_{\rm Bol}/L_{\rm Edd}$. We find that there is no correlation between $M_{\rm BH}$ and PC2 no matter at low luminosity or high luminosity. It is suggested that there exists the BLRs orientation effect to derive the BLR velocity from FWHM (Shen & Ho 2014). In Fig. 8, we divide low-z PG QSOs into two parts at $\mathrm{FWHM(H}\beta) = 3000\ \mathrm{km\ s^{-1}}$. For low-FWHM part, PC1 has a strong correlation with $M_{\rm BH}$ and a weak correlation with $L_{\rm Bol}/L_{\rm Edd}$. PC2 has weak correlations with $M_{\rm BH}$ and $L_{\rm Bol}/L_{\rm Edd}$. For high-FWHM part, PC1 still has very weak correlations with $M_{\rm BH}$ and $L_{\rm Bol}/L_{\rm Edd}$. PC2 has strong correlations with $M_{\rm BH}$ and $L_{\rm Bol}/L_{\rm Edd}$. The dividing with FWHM affects seriously the correlations between PC1 and $M_{\rm BH}$ and $L_{\rm Bol}/L_{\rm Edd}$. Because PC1 has a strong correlation with Hβ FWHM, dividing PG QSOs based on Hβ FWHM would lead to narrower PC1 parameter space, which would lead to weaken PC1 correlation with $M_{\rm BH}$ and $L_{\rm Bol}/L_{\rm Edd}$. PC2 also has a strong correlation with continuum luminosity, dividing PG QSOs based on the luminosity would lead to narrower PC2 parameter space, which would lead to weaken PC2 correlation with $M_{\rm BH}$ and $L_{\rm Bol}/L_{\rm Edd}$. Therefore, considering the PG QSOs subsample with different radio loudness, continuum luminosity, and Hβ FWHM, the narameter range limitation will change the strongness of the relations between PC1/PC2 and $M_{\rm BH}$, $L_{\rm Bol}/L_{\rm Edd}$. Large sample with larger parameter coverage is needed for this kind of work in the future.

Since PC1/PC2 has a correlation with $M_{\rm BH}$ or $L_{\rm Bol}/L_{\rm Edd}$, in Fig. 9, we show the relationship between C IV EW and PC1/PC2. The C IV EW has a strong correlation with PC1 and the correlation with PC2 is a little weaker. Excluding RL QSOs and BAL QSOs, these correlations become stronger. From PCA shown in Boroson (2002), PC1 has a strong correlation with the Fe II strength, $R_{\rm Fe}$ (the ratio of optical Fe II and Hβ EW). We find C IV EW also has a strong correlation with $R_{\rm Fe}$ with $r = -0.59$.

3.4 Physical driver of the Baldwin effect of C IV

For low-z PG QSOs, Baskin & Laor (2004) found that the C IV Baldwin effect is weak. Fig. 10 shows the C IV Baldwin effect for our low-z and high-z QSOs sample. For the 81 low-z PG QSOs subsample, the C IV Baldwin effect is weak, with $r = -0.15$. It is consistent with the result by Baskin & Laor (2004). Considering the speciality of RL QSOs and BAL QSOs, we exclude 16 RL QSOs and 5 BAL QSOs, and find that the C IV Baldwin effect becomes stronger with $r = -0.25$. For high-z QSOs subsample, the C IV Baldwin effect is stronger than low-z PG QSOs subsample with $r = -0.34$. Excluding 12 RL QSOs, 7 BAL QSOs and 11 weak line QSOs in high-z subsample, the C IV Baldwin effect becomes stronger with $r = -0.45$. For the total sample, we find there exists a C IV Baldwin effect with $r = -0.3$, which is consistent with the result by Bian et al. (2012) from 35019 QSOs in SDSS DR7. We notice that, for the total sample, excluding RL QSOs, BAL QSOs, and weak line QSOs, the correlation coefficient in C IV Baldwin effect doesn't increase.

For the high-z, we calculate the SMBH $M_{\rm BH}$ and $L_{\rm Bol}/L_{\rm Edd}$ using the same Hβ emission line as that for low-z PG QSOs. Fig.

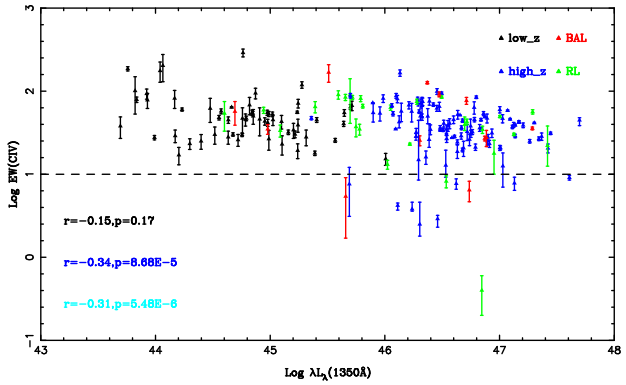

Figure 10. The C IV Baldwin effect, i.e., the C IV EW versus the UV continuous luminosity at 1350Å for our sample of low-z and high-z QSOs. Black triangles denote 81 PG QSOs with low redshift ($z < 0.5$), and blue triangles denote SDSS QSOs ($1.5 < z < 5$). Red triangles denote BAL QSOs and green triangles denote RL QSOs.

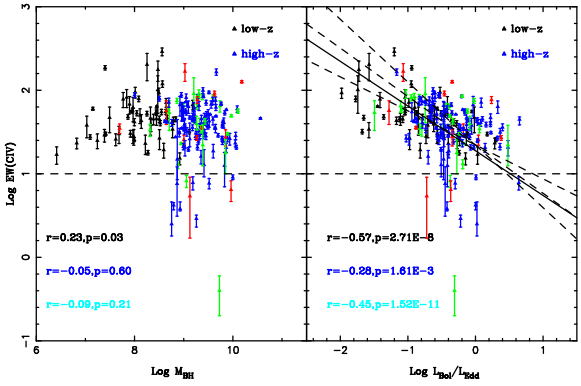

Figure 11. Left: the relationship between C IV EW and $M_{\rm BH}$. Right: the relationship between C IV EW and $L_{\rm Bol}/L_{\rm Edd}$. The marks are the same as Fig. 10. The solid line is the best linear fitting of BCES bisector for the low-z sample. The dotted lines are the best fitting of BCES bisector for the entire sample with 2σ. BAL QSOs, RL QSOs and weak line QSOs are excluded from the entire sample during the fitting.

11 shows C IV EW versus $M_{\rm BH}$ (left-hand panel) and $L_{\rm Bol}/L_{\rm Edd}$ (right-hand panel). For low-z PG QSOs subsample, there is a weak correlation between C IV EW and $M_{\rm BH}$ with $r = -0.23$ and $P_{\rm null} = 0.03$. However, for high-z QSOs subsample or the total sample, the correlations become weaker with $r = -0.05$, $P_{\rm null} = 0.60$ and $r = -0.09$, $P_{\rm null} = 0.21$, respectively. For low-z PG QSOs subsample, C IV EW has a strong correlation with $L_{\rm Bol}/L_{\rm Edd}$ with $r = -0.57$, which is consistent with the result by (Baskin & Laor 2004). For the high-z subsample, the relation becomes weaker with r=-0.28. For the total sample, C IV EW has a strong correlation with $r = -0.45$, $P_{\rm null} = 1.52 \times 10^{-11}$. The correlation still exists when excluding RL QSOs, BAL QSOs and weak line QSOs. For the relation between C IV EW and $L_{\rm Bol}$(i.e., $\lambda L_\lambda(5100\text{Å})$), we find r=-0.15, -0.23, -0.27 for low-z, high-z, total sample, respectively. Considering that the correlation between C IV EW and $L_{\rm Bol}/L_{\rm Edd}$ is stronger than the relation between C IV EW and $M_{\rm BH}$, and the C IV Baldwin effect, the Eddington ratio seems to be a better underlying physical parameter than the central SMBH $M_{\rm BH}$ in C IV Baldwin effect. Considering intrinsic scatter of 0.3 dex in $L_{\rm Bol}/L_{\rm Edd}$, we use the bivariate correlated errors and scatter method (BCES; Akritas et la. 1996) to perform the linear regression (Table. 3). The BCES Bisector best-fitting relation for low-z PG QSOs subsample is,

$$\log \mathrm{EW(C\,IV)} = (-0.53 \pm 0.10)\log(\lambda \mathrm{L}_\lambda(5100\text{Å})) + (1.28 \pm 0.08) \quad (4)$$

is plotted as the solid line in Fig. 11. The high-z QSOs follow the solid line found in low-z PG QSOs subsample. Some of weak line QSOs deviated from the above fitting line. Considering the contamination in C IV EW measurement for BAL QSOs, and the jet effect in mass calculation for RL QSOs, we exclude RL QSOs, BAL QSOs and weak line QSOs, a new BCES Bisector best-fitting relation for the total QSOs sample is,

$$\log \mathrm{EW(C\,IV)} = (-0.58 \pm 0.09)\log(\lambda \mathrm{L}_\lambda(5100\text{Å})) + (1.35 \pm 0.05) \quad (5)$$

is plotted as the dash lines with 2σ in the slope in Fig. 11. It is consistent with the result by Shemmer & Lieber (2015). The slope of -0.56 is steeper than the slope of -0.268 found by Bian et al. (2012) with the Mg II -based $L_{\rm Bol}/L_{\rm Edd}$. For RL QSOs, BAL QSOs and weak line QSOs, the C IV Baldwin effect, as well as the $L_{\rm Bol}/L_{\rm Edd}$ origin, need to be investigated in larger sample with reliable C IV EW, the UV continuum luminosity, $M_{\rm BH}$ and $L_{\rm Bol}/L_{\rm Edd}$.

4 CONCLUSIONS

We compile a sample of 87 low-z and 126 high-z QSOs across the widest possible ranges of redshift ($0 < z < 5$) with available Hβ and C IV observations. The Hβ -based single-epoch SMBH $M_{\rm BH}$ and $L_{\rm Bol}/L_{\rm Edd}$ are consistently calculated for QSOs from low-z to high-z, which is used to investigate the underlying driver for the C IV Baldwin effect. The main conclusions can be summarized as follows.

(1) An empirical formula is presented to estimate the host correction in the continuum luminosity at 5100Å. For low-z PG QSOs, the estimated host fraction is less than 50%. For 87 low-z and 126 high-z QSOs, the Hβ -based single-epoch SMBH $M_{\rm BH}$ and $L_{\rm Bol}/L_{\rm Edd}$ are consistently calculated.

(2) Considering PC1/PC2 from optical PCA, it is found that PC1 has strong correlations with $M_{\rm BH}$ and $L_{\rm Bol}/L_{\rm Edd}$. PC2 has a strong correlation with $M_{\rm BH}$ and a weak correlation with $L_{\rm Bol}/L_{\rm Edd}$. It suggests that $L_{\rm Bol}/L_{\rm Edd}$ is the main driver of PC1, which is consistent with Boroson (2002). For low-z PG QSOs, C IV EW has a relatively weak correlation with the continuum luminosity at 1350 Å. The C IV EW has a strong correlation with the optical Fe II strength or PC1.

(3) For low-z PG QSOs subsample, excluding the RL QSOs and BAL QSOs, the C IV Baldwin effect becomes stronger. For low-z and high-z sample, there exists a C IV Baldwin effect with $r = -0.3$, which is consistent with the result by Bian et al. (2012) from 35019 QSOs in SDSS DR7. For the total sample, the correlation between C IV EW and Hβ -based $M_{\rm BH}$ is very weak, and C IV EW has a strong correlation with $L_{\rm Bol}/L_{\rm Edd}$. The Eddington ratio seems to be a better underlying physical parameter than the SMBH $M_{\rm BH}$ in C IV Baldwin effect. For RL QSOs, BAL QSOs and weak line QSOs, the C IV Baldwin effect, as well as the $L_{\rm Bol}/L_{\rm Edd}$ origin, need to be investigated in larger sample.

5 ACKNOWLEDGEMENTS

We are very grateful to the anonymous referee for her/his instructive comments which improved the content of the paper. This work has been supported by the National Science Foundations of China (Nos. 11373024, 11173016 and 11233003).

REFERENCES

Akritas M. G., & Bershady M. A., 1996, ApJ, 470, 706
Assef R. J., et al., 2011, ApJ, 742, 93
Bachev R., Marziani P., Sulentic J. W., et al., 2004, ApJ, 617, 171
Baldwin J. A., 1977, ApJ, 214, 679
Baskin A., & Laor A., 2004, MNRAS, 350, 31
Bentz, M. C., et al., 2013, ApJ, 767, 149
Bian W. H., Zhao Y. H., 2004, MNRAS, 347, 607
Bian W. H., et al., 2012, MNRAS, 427, 2881
Bian W. H., et al., 2014, MNRAS, 456, 4081
Boroson A. T., & Green R. F., 1992, ApJS, 80, 109
Boroson T. A., 2002, ApJ, 565, 78
Brandt W. N., Laor A., & Wills B. J., 2000, ApJ, 528, 637
Dietrich M., Hamann F., Shields J. C., Constantin, A., Vestergaard, M., Chaffee, F., Foltz, C. B., & Junkkarinen, V. T., 2002, ApJ, 581, 912
Dietrich M., et al. 2009, ApJ, 696, 1998
Du Pu., et al., 2015, ApJ, 806, 22
Du Pu., et al., 2016, ApJ, 818, L14
Green P. J., Forster K., & Kuraszkiewicz J., 2001, ApJ, 556, 727
Greene J. E. & Ho L. C., 2005, ApJ, 630, 122
Ho L. C., et al., 2012, ApJ, 754, 11(H12)
Jester S., Schneider D. P., Richards G. T., et al., 2005, AJ, 130, 873
Jun H. D., et al., 2015, ApJ, 806, 109 (J15)
Kaspi S., Smith P.S., Netzer H., Maoz D.,Jannuzi B.T., Giveon U., 2000, ApJ, 533, 631
Laor A., 1998, ApJ, 505, L83
Netzer H., et al., 2007, ApJ, 671, 1256
Netzer H., Laor, A., & Gondhalekar P. M., 1992, MNRAS, 254, 15
Neugebauer G., et al., 1987, ApJS, 63, 615
Peng C. Y., Ho, L. C., Impey C. D., Rix, H., 2002, AJ, 124, 266
Peterson B. M., Ferrarese L., Gilbert K. M. et al., 2004, ApJ, 613, 682
Press W. H., Teukolsky S. A., Vetterling W. T., & Flannery B. P., 1992, Numerical Recipes in FORTRAN. The Art of Scientific Computing (2nd ed.; Cambridge: Cambridge Univ. Press), 660
Rafiee A., Hall P. B., 2011, MNRAS, 415, 2932
Richards G. T., et al. 2006, ApJS, 166, 470
Richards G. T., et al. 2011, AJ, 141, 167
Schmidt M. & Green R. F., 1983, ApJ, 269, 352
Shang Z., Wills B. J., Robinson E. L., Wills D., Laor A., Xie B., & Yuan J., 2003, ApJ, 586, 52
Shemmer O., et al., 2004, ApJ, 614, 547 (S04)
Shemmer O. & Lieber S., 2015, ApJ, 805, 124
Shen Y., et al., 2011, ApJS, 194, 45
Shen Y., & Liu X., 2012, ApJ, 753, 125 (SY12)
Shen Y., & Ho L. C., 2014, Nature, 513, 210
Shen Y., Horne K., Grier C. J., et al. 2016, ApJ, 818, 30, arXiv:1510.02802
Shi Y., Rieke G. H., Ogle P. M., et al., 2014, ApJS, 214, 23
Shields J. C., 2007, in Ho L. C., Wang J-M., eds, ASP Conf. Ser. Vol. 373, The Central Engine of Active Galactic Nuclei. Astron. Soc. Pac., San Francisco, p. 355
Simcoe R. A., et al., 2010, SPIE Conf., 7735, 38
Vestgaard M., & Peterson B. M., 2006, ApJ, 641, 689 (VP06)
Wills B. J., Laor A., Brotherton M. S., Wills D., Wilkes B. J., Ferland G. J., Shang Z., 1999, ApJ, 515, L53
Wilson J. C., et al., 2004, SPIE Conf., 5492, 1295
Wu J., et al., 2009, ApJ, 702, 767
Xu Y., Bian W. H., Yuan Q. R., Huang K., L., 2008, MNRAS, 389, 1703

Table 1. The properties of 87 PG QSOs. Col.(1): Sequence number; Col.(2): Name of PG QSOs, and the superscript of ^{a} in the Col. (2) indicates the reverberation mapping objects; Col.(3): Redshift from (Schmidt & Green 1983); Col.(4): The continuum luminosity at 1350Å in units of erg/s (in logarithm scale); Col.(5): The equivalent widths of C IV in units of Å; Col.(6): The ratio of the equivalent widths of Fe II (4434-4684Å) and Hβ ; Col.(7-8): The continuum luminosity at 5100 Å (Vestergaard & Peterson 2006; Neugebauer et al. 1987; Schmidt & Green 1983) and the host corrected luminosity at 5100Å, in units of erg/s (in logarithm scale); Col.(8): The host corrected continuum luminosity at 5100 Å, in units of erg/s (in logarithm scale); Col.(9): The Hβ FWHM in units of km s^{-1} (Vestergaard & Peterson 2006); Col.(10, 11, 12): The host-corrected $M_{\rm BH}$ in this work (all in logarithm scale), the $M_{\rm BH}$ from other works (Vestergaard & Peterson 2006; Baskin & Laor 2004); Col.(13): The host-corrected Eddington ratio (in logarithm scale); Col.(14): The radio loudness (in logarithm scale); Col.(15, 16): Eigenvector 1 and Eigenvector 2 of optical PCA.

N	Name	z	L_{1350} (erg s^{-1})	EW(C IV) (Å)	$R_{\rm FeII}$	L_{5100} (erg s^{-1})	$L_{5100,cor}$ (erg s^{-1})	FWHM$_{\rm H\beta}$ (km s^{-1})	$M_{\rm BH,cor}$ ($M_\odot$)	$M_{\rm BH,VP}$ ($M_\odot$)	$M_{\rm BH,BL}$ ($M_\odot$)	$L_{\rm Bol}/L_{\rm Edd}$	R	$pc1$	$pc2$
(1)	(2)	(3)	(4)	(5)	(6)	(7)	(8)	(9)	(10)	(11)	(12)	(13)	(14)	(15)	(16)
1	0003+158	0.450	46.050	63.5 ± 4.6	0.00	46.018	46.018	4750.7	9.273	9.273	9.055	-0.388	2.24	3.409	-0.796
2	$0003+199^a$	0.025	44.232	60.1 ± 2.6	0.62	44.160	43.720	1585.0	7.152	7.152	7.220	-0.566	-0.57	-1.896	1.860
3	0007+106	0.089	44.943	59.0 ± 5	0.35	44.816	44.734	5084.6	8.689	8.731	8.561	-1.089	2.29	2.302	0.188
4	$0026+129^a$	0.142	45.240	19.3 ± 3.9	0.51	45.100	44.910	1821.0	8.594	8.594	7.833	-0.818	0.03	0.574	-0.248
5	0043+039	0.384	45.658	5.4 ± 3.7	1.18	45.537	45.537	5290.8	9.126	9.126	8.952	-0.722	-0.92	-2.112	-2.484
6	0049+171	0.064	44.064	203.0 ± 73	0.00	44.004	43.813	5234.3	8.254	8.350	8.146	-1.575	-0.49	2.492	2.700
7	0050+124	0.061	44.755	29.9 ± 1.5	1.47	44.794	44.709	1171.4	7.402	7.444	7.238	0.173	-0.48	-2.163	-0.627
8	$0052+251^a$	0.155	45.277	119.0 ± 10.5	0.23	45.030	44.750	5187.0	8.567	8.567	8.745	-0.951	-0.62	1.649	0.816
9	0157+001	0.164	45.099	43.0 ± 8	0.71	44.975	44.911	2431.9	8.137	8.169	8.006	-0.360	0.33	0.718	0.594
10	$0804+761^a$	0.100	45.406	45.0 ± 3	0.67	45.060	44.850	3045.0	8.841	8.841	8.352	-1.125	-0.22	-0.593	-0.651
11	0838+770	0.131	44.852	50.0 ± 10	0.89	44.727	44.634	2763.8	8.110	8.157	7.992	-0.610	-0.96	-1.628	-0.060
12	$0844+349^a$	0.064	44.634	28.0 ± 5	0.89	44.490	44.367	2386.0	7.966	7.966	7.759	-0.733	-1.52	-2.101	0.629
13	$0921+525^a$	0.035	43.758	186.0 ± 11	0.14	43.630	43.590	2079.0	7.400	7.400	7.206	-0.944	0.17	0.539	2.775
14	0923+129	0.190	43.923	93.0 ± 13	0.53	43.860	43.647	7598.4	8.495	8.601	7.233	-1.982	-0.85	-0.756	1.260
15	0923+201	0.029	45.314	28.0 ± 6	0.72	45.038	44.981	1956.7	7.984	8.012	9.094	-0.136	0.32	-0.129	-0.003
16	0934+013	0.050	–	–	0.48	43.875	43.664	1254.3	6.939	7.044	–	-0.409	-0.42	-0.838	3.188
17	0947+396	0.206	44.975	55.0 ± 4	0.23	44.808	44.725	4816.7	8.638	8.679	8.530	-1.047	-0.60	0.981	1.244
18	$0953+414^a$	0.239	45.646	54.9 ± 5	0.25	45.400	45.130	3111.0	8.441	8.441	8.488	-0.445	-0.36	0.800	-0.734
19	1001+054	0.161	44.979	34.9 ± 4.6	0.82	44.741	44.650	1699.8	7.696	7.741	7.645	-0.180	-0.30	-2.452	-1.449
20	1004+130	0.240	–	–	0.23	45.536	45.536	6290.4	9.275	9.275	–	-0.873	2.36	0.818	-3.485
21	1011-040	0.058	44.398	25.0 ± 5	0.73	44.259	44.105	1381.0	7.243	7.320	7.190	-0.272	-1.00	-2.225	0.682
22	1012+008	0.185	45.104	23.0 ± 6	0.66	45.011	44.951	2614.7	8.220	8.250	8.069	-0.403	-0.30	-0.145	-0.549
23	1022+519	0.045	43.694	38.0 ± 11	1.08	43.696	43.456	1566.4	7.028	7.148	6.940	-0.706	-0.64	-3.002	2.245
24	1048-090	0.344	45.697	91.0 ± 50	0.09	45.596	45.596	5610.8	9.206	9.206	9.022	-0.744	-1.00	2.683	-1.268
25	1048+342	0.167	44.908	46.0 ± 17	0.32	44.708	44.613	3580.9	8.324	8.372	8.241	-0.845	2.58	0.559	-0.192
26	1049-005	0.357	45.713	67.0 ± 8.8	0.56	45.633	45.633	5350.6	9.183	9.183	8.989	-0.684	-0.60	2.174	-0.323
27	1100+772	0.313	45.717	84.0 ± 4.9	0.21	45.575	45.575	6151.2	9.275	9.275	9.112	-0.834	2.51	3.756	-0.652
28	1103-006	0.425	45.748	37.2 ± 9	0.60	45.667	45.667	6182.6	9.326	9.326	9.132	-0.793	2.43	1.681	-1.915
29	1114+445	0.144	44.842	55.0 ± 4.1	0.20	44.734	44.642	4554.4	8.548	8.594	8.415	-1.040	-0.89	-0.065	-0.203
30	1115+407	0.154	44.720	25.9 ± 4.2	0.54	44.619	44.513	1678.8	7.616	7.669	7.505	-0.237	-0.77	-1.291	-0.116
31	1116+215	0.177	45.641	40.5 ± 2.9	0.47	45.397	45.378	2896.9	8.523	8.532	8.425	-0.279	-0.14	0.006	-1.223
32	1119+120	0.049	44.172	29.0 ± 5	0.90	44.132	43.960	1772.9	7.387	7.473	7.280	-0.561	-0.82	-1.677	1.584
33	1121+422	0.234	44.979	41.7 ± 4.1	0.37	44.883	44.808	2192.3	7.996	8.033	7.856	-0.322	-1.00	-0.921	0.710
34	1126-041	0.060	44.517	30.0 ± 7	1.07	44.385	44.248	2111.1	7.683	7.752	7.598	-0.569	-0.77	-2.181	-0.279
35	1149-110	0.049	44.167	82.0 ± 20	0.36	44.107	43.931	3032.2	7.839	7.927	7.729	-1.042	-0.06	0.001	2.565
36	1151+117	0.176	44.988	26.6 ± 7.1	0.24	44.756	44.666	4284.3	8.507	8.552	8.435	-0.975	-1.15	-0.355	-0.321
37	1202+281	0.165	44.763	290.0 ± 31.3	0.29	44.601	44.492	5036.4	8.560	8.615	8.462	-1.202	-0.72	1.745	0.468
38	1211+143	0.085	45.236	55.7 ± 1.8	0.52	45.071	45.018	1816.9	7.938	7.964	7.831	-0.053	-0.87	-0.302	-0.316
39	1216+069	0.334	45.700	64.5 ± 4.4	0.20	45.721	45.721	5179.9	9.199	9.199	8.954	-0.612	0.22	1.117	-1.401
40	$1226+023^a$	0.158	46.218	23.0 ± 0.7	0.57	46.020	45.900	3500.0	8.947	8.947	8.876	-0.181	3.06	1.193	-2.548
41	$1229+204^a$	0.064	44.554	48.0 ± 3	0.59	44.390	43.640	3335.0	7.865	7.865	8.004	-1.359	-0.96	-0.861	0.804
42	1244+026	0.048	44.204	17.0 ± 4	1.20	43.801	43.578	720.6	6.414	6.526	6.614	0.030	-0.28	-3.500	2.584
43	1259+593	0.472	46.007	15.3 ± 2.5	1.27	45.906	45.906	3377.3	8.920	8.920	8.738	-0.148	-1.00	-2.105	-2.117
44	1302-102	0.286	46.023	13.1 ± 1.6	0.19	45.827	45.827	3383.4	8.882	8.882	8.749	-0.189	2.27	1.885	-1.579
45	$1307+085^a$	0.155	45.244	71.2 ± 8.5	0.19	45.010	44.790	5307.0	8.643	8.643	8.541	-0.987	-1.00	1.384	0.342
46	1309+355	0.184	45.088	33.5 ± 5.5	0.28	45.014	44.954	2917.3	8.317	8.347	8.155	-0.497	1.26	1.441	-0.906
47	1310-108	0.035	43.930	78.0 ± 16	0.38	43.725	43.490	3606.0	7.769	7.887	7.759	-1.413	-1.00	0.751	4.280
48	1322+659	0.168	45.020	52.6 ± 3.4	0.59	44.980	44.917	2765.4	8.252	8.284	8.076	-0.469	-0.92	-0.992	0.850
49	1341+258	0.087	44.477	62.0 ± 20	0.38	44.344	44.202	3013.9	7.969	8.040	7.878	-0.901	-0.92	-0.742	1.268
50	1351+236	0.055	43.822	101.0 ± 48	1.18	44.048	43.864	6527.2	8.471	8.563	8.216	-1.741	-0.59	-0.702	0.547
51	1351+640	0.087	44.953	43.3 ± 4.4	0.24	44.835	44.755	5646.1	8.791	8.831	8.656	-1.170	0.64	1.443	0.897
52	1352+183	0.158	45.024	45.1 ± 6.5	0.46	44.816	44.734	3580.6	8.385	8.426	8.299	-0.785	-0.96	-0.381	0.106
53	1354+213	0.300	–	–	0.31	44.977	44.913	4126.7	8.598	8.630	–	-0.818	-1.10	1.282	0.375
54	1402+261	0.164	45.217	30.3 ± 2.8	1.23	44.983	44.920	1873.7	7.915	7.947	7.845	-0.129	-0.64	-2.466	-0.714
55	1404+226	0.098	44.299	23.3 ± 3.4	1.01	44.379	44.242	787.3	6.823	6.892	6.713	0.285	-0.33	-3.123	-0.929
56	$1411+442^a$	0.089	44.693	56.9 ± 18	0.49	44.620	44.500	2640.0	8.646	8.646	7.874	-1.280	-0.89	-1.150	-0.365
57	1415+451	0.114	44.572	57.3 ± 3.9	1.25	44.561	44.447	2591.2	7.961	8.018	7.797	-0.647	-0.77	-3.045	-0.211
58	1416-129	0.129	45.510	168.1 ± 40.2	0.18	45.135	45.089	6098.0	9.025	9.048	9.002	-1.070	0.06	2.186	-0.667
59	1425+267	0.366	45.392	64.8 ± 10	0.11	45.761	45.761	9404.7	9.737	9.737	9.317	-1.110	1.73	3.763	-1.448
60	$1426+015^a$	0.086	45.158	32.0 ± 2	0.39	44.880	44.570	6808.0	9.113	9.113	8.921	-1.677	-0.55	0.289	0.434

Table 1. – continue

N (1)	Name (2)	z (3)	L_{1350} (4)	EW(C IV) (5)	$R_{\rm FeII}$ (6)	L_{5100} (7)	$L_{5100,cor}$ (8)	FWHM$_{\rm H\beta}$ (9)	$M_{\rm BH,cor}$ (10)	$M_{\rm BH,VP}$ (11)	$M_{\rm BH,BL}$ (12)	$L_{\rm Bol}/L_{\rm Edd}$ (13)	R (14)	$pc1$ (15)	$pc2$ (16)
61	1427+480	0.221	44.988	53.2 ± 3.7	0.36	44.759	44.670	2515.3	8.046	8.091	7.978	-0.510	-0.80	0.770	0.892
62	1435-067	0.129	45.242	39.0 ± 7	0.45	44.918	44.847	3156.9	8.332	8.368	8.300	-0.619	-1.15	-0.732	-0.160
63	1440+356	0.077	44.676	30.1 ± 1.4	1.19	44.546	44.430	1393.5	7.413	7.471	7.335	-0.117	-0.43	-1.874	0.401
64	1444+407	0.267	45.390	17.9 ± 1.1	1.45	45.203	45.164	2456.5	8.273	8.292	8.158	-0.242	-1.10	-2.562	-1.225
65	1448+273	0.065	–	–	0.90	44.482	44.358	814.7	6.911	6.973	–	0.313	-0.60	-1.876	0.758
66	1501+106	0.036	44.664	64.0 ± 1	0.35	44.285	44.135	5454.1	8.451	8.526	8.482	-1.450	-0.44	1.255	1.827
67	1512+370	0.371	45.656	84.3 ± 7.2	0.00	45.602	45.602	6802.7	9.376	9.376	9.168	-0.908	2.28	3.934	-0.923
68	1519+226	0.137	44.820	68.0 ± 16	1.01	44.710	44.615	2187.3	7.897	7.945	7.777	-0.416	-0.05	-2.021	-0.221
69	1534+580	0.030	43.836	79.0 ± 6	0.27	43.687	43.445	5323.5	8.085	8.206	8.047	-1.774	-0.15	1.690	4.678
70	1535+547	0.038	43.991	27.6 ± 1.7	0.47	43.961	43.764	1420.4	7.097	7.195	7.010	-0.467	-0.85	-2.801	0.279
71	1543+489	0.400	45.567	25.6 ± 1.4	0.86	45.445	45.431	1529.2	7.995	8.001	7.844	0.303	-0.82	-2.791	-1.797
72	1545+210	0.266	45.594	90.5 ± 10.5	0.00	45.428	45.413	7021.7	9.309	9.317	9.165	-1.030	2.62	3.654	-1.141
73	1552+085	0.119	44.758	47.0 ± 16	1.02	44.704	44.608	1377.0	7.492	7.540	7.364	-0.018	-0.35	-2.872	-0.730
74	1612+261	0.131	44.872	94.6 ± 13.9	0.18	44.717	44.623	2490.9	8.014	8.061	7.913	-0.525	0.45	2.143	1.693
75	$1613+658^a$	0.129	44.849	54.0 ± 3	0.38	44.840	44.710	8441.0	8.446	8.446	8.953	-0.870	0.00	2.061	0.205
76	$1617+175^a$	0.114	45.203	34.0 ± 7	0.60	44.850	44.330	5316.0	8.774	8.774	8.729	-1.578	-0.14	-0.199	-0.758
77	1626+554	0.133	44.785	45.6 ± 7.6	0.32	44.580	44.469	4473.8	8.446	8.501	8.371	-1.111	-0.96	0.127	0.720
78	$1700+518^a$	0.292	–	–	1.42	45.680	45.530	2185.0	8.893	8.893	–	-0.497	0.37	-3.505	-3.873
79	1704+608	0.371	45.779	34.8 ± 5.2	0.00	45.702	45.702	6552.4	9.394	9.394	9.198	-0.826	2.81	5.905	-0.594
80	2112+059	0.466	46.304	25.5 ± 3.5	0.63	46.181	46.181	3176.4	9.004	9.004	8.834	0.043	-0.49	-0.988	-2.688
81	$2130+099^a$	0.061	44.792	47.0 ± 3	0.64	44.540	44.140	2294.0	8.660	8.660	7.805	-1.654	-0.49	-0.487	0.919
82	2209+184	0.070	44.601	54.0 ± 21	0.44	44.469	44.344	6487.5	8.706	8.769	8.601	-1.496	2.15	0.570	-0.599
83	2214+139	0.067	44.635	45.0 ± 4	0.32	44.662	44.561	4532.0	8.503	8.554	8.308	-1.076	-1.30	-1.662	-1.135
84	2233+134	0.325	–	–	0.89	45.327	45.301	1709.2	8.026	8.039	–	0.141	-0.55	-1.320	-1.086
85	2251+113	0.323	45.807	66.0 ± 3.5	0.32	45.692	45.692	4147.2	8.992	8.992	8.816	-0.433	2.56	1.857	-2.137
86	2304+042	0.042	44.040	176.0 ± 48	0.09	44.066	43.884	6486.8	8.476	8.567	8.320	-1.726	-0.60	0.467	2.736
87	2308+098	0.432	45.789	81.5 ± 6.8	0.00	45.777	45.777	7914.3	9.595	9.595	9.372	-0.952	2.27	3.539	-1.259

Table 2. The properties of high-z QSOs. Col.(1): Sequence number; Col.(2): Name of high-z QSOs; Col.(3): Redshift; Col.(4): The continuum luminosity at 1350 Åin units of erg s^{-1} (in logarithm scale); Col.(5): The equivalent widths of C IV in units of Å; Col.(6): The continuum luminosity at 5100Åin units of erg s^{-1} (in logarithm scale); Col.(7): The Hα and Hβ FWHM in units of km s^{-1} ; Col.(8): Reference. A11: (Assef et la. 2011), H12: (Ho et al. 2012), J15: (Jun et al. 2015), N07: (Netzer et al. 2007), S04: (Shemmer et al. 2004), S15: (Shemmer & Lieber 2015), Sy12: (Shen & Liu 2012). The number of objects in each literature is 7, 1, 26,15, 10, 7, 60 respectively. Col.(9): The single-epoch Hβ -based SMBH mass; Col.(10): The Eddington ratio; Col.(11): The radio loudness in logarithm scale (Shen et al. 2011).

N	Name	z	L_{1350} (erg s^{-1})	EW(C IV) (Å)	L_{5100} (erg s^{-1})	FWHM($H\alpha$, $H\beta$) (km s^{-1})	ref.	$M_{\rm BH}$ ($M_{\odot}$)	L_{Bol}/L_{Edd}	R
(1)	(2)	(3)	(4)	(5)	(6)	(7)	(8)	(9)	(10)	(11)
1	SDSS225800.02-084143	1.494	46.585	27.479	45.84	(–, 3188)	sy12	8.835	-0.133	–
2	SDSS035856.73-054023	1.506	46.273	31.912 ± 3.737	45.80	(–, 4240)	sy12	9.065	-0.398	–
3	SDSS081331.28+254503	1.51	47.169	42.45 ± 1.396	46.96	(–, 5091)	sy12	9.802	0.021	–
4	HS0810+2554	1.51	47.169	42.45 ± 1.396	44.84	(–, 4400)	A11	8.617	-0.911	–
5	SDSS133321.90+005824	1.514	46.455	99.303 ± 7.916	45.90	(–, 5841)	sy12	9.391	-0.628	–
6	SDSS152111.86+470539	1.516	46.475	65.392 ± 8.13	45.97	(–, 5100)	sy12	9.312	-0.472	–
7	FBQ1633+3134	1.518	46.677	19.631 ± 1.034	45.72	(–, 4600)	A11	9.096	-0.509	–
8	SDSS085543.26+002908	1.523	46.109	80.674 ± 8.211	45.78	(–, 5518)	sy12	9.284	-0.637	–
9	SDSS123355.21+031327	1.526	46.329	74.82 ± 7.72	45.93	(–, 7227)	sy12	9.591	-0.798	–
10	SDSS104910.31+143227	1.536	46.299	56.828 ± 2.845	46.01	(–, 3629)	sy12	9.036	-0.157	–
11	SDSS143230.57+012435	1.538	46.513	40.896 ± 3.845	45.97	(–, 2699)	sy12	8.755	0.077	–
12	SDSS154212.90+111226	1.538	46.635	52.345 ± 6.235	46.06	(–, 6028)	sy12	9.498	-0.577	–
13	SDSSJ105023.68-01055	1.539	45.69	7.607 ± 4.494	45.55	(3891, 4798)	H12	8.865	-0.449	–
14	SDSS081344.15+152221	1.541	46.537	30.334 ± 3.931	46.03	(–, 5403)	sy12	9.391	-0.494	–
15	SDSS082146.22+571226	1.542	46.75	30.836 ± 3.051	46.31	(–, 4804)	sy12	9.429	-0.251	–
16	SDSS074029.82+281458	1.543	46.495	94.255 ± 3.388	46.04	(–, 6190)	sy12	9.514	-0.607	–
17	SDSS015733.87-004824	1.545	46.358	16.088 ± 2.94	45.79	(–, 5953)	sy12	9.352	-0.7	–
18	SDSS123442.16+052126	1.549	46.565	40.881 ± 5.644	46.16	(–, 8173)	sy12	9.816	-0.787	–
19	SDSS101447.54+521320	1.55	46.55	38.6 ± 5.77	46.02	(–, 3534)	sy12	9.015	-0.132	–
20	SDSS135439.70+301649	1.55	46.31	49.973 ± 5.56	46.10	(–, 5666)	sy12	9.465	-0.502	–
21	SDSS171030.20+602347	1.552	46.453	62.286 ± 5.034	46.13	(–, 6924)	sy12	9.655	-0.66	–
22	SDSS223246.80+134702	1.555	46.423	68.885 ± 3.261	46.06	(–, 8146)	sy12	9.762	-0.836	–
23	SDSS100930.51+023052	1.556	45.985	81.689 ± 8.522	45.59	(–, 4721)	sy12	9.051	-0.599	–
24	SDSS124006.70+474003	1.559	46.279	74.844 ± 5.32	45.98	(–, 3038)	sy12	8.864	-0.020	41.14
25	SDSS093318.49+141340	1.562	46.388	75.518 ± 7.676	46.10	(–, 6992)	sy12	9.649	-0.683	–
26	SDSS113829.33+040101	1.564	46.738	26.227 ± 4.187	46.09	(–, 9814)	sy12	9.937	-0.984	–
27	SDSS084451.91+282607	1.57	46.314	71.545 ± 9.017	45.92	(–, 2599)	sy12	8.698	0.085	–
28	SDSS094126.49+044328	1.571	46.291	71.17 ± 4.79	45.85	(–, 6441)	sy12	9.455	-0.735	–
29	SDSS081227.19+075732	1.575	46.539	26.639 ± 2.516	46.00	(–, 9813)	sy12	9.895	-1.026	–
30	SDSS204538.96-005115	1.589	46.324	48.858 ± 4.253	45.84	(–, 4721)	sy12	9.18	-0.470	–
31	SDSS014705.42+133210	1.59	46.718	32.601 ± 7.143	46.21	(–, 4506)	sy12	9.321	-0.248	–
32	SDSS091754.44+043652	1.59	46.132	165.696 ± 14.534	45.63	(–, 9310)	sy12	9.664	-1.166	–
33	SDSS114023.40+301651	1.592	46.891	47.193 ± 5.803	46.42	(–, 4463)	sy12	9.421	-0.132	–
34	SDSS125140.82+080718	1.596	46.747	37.971 ± 8.129	46.09	(–, 3389)	sy12	9.016	-0.058	–
35	SDSS104603.22+112828	1.602	46.234	56.916 ± 14.337	45.87	(–, 4768)	sy12	9.2	-0.467	–
36	SDSS204009.62-065402	1.61	45.957	54.143 ± 10.508	45.46	(–, 4770)	sy12	8.997	-0.671	–
37	SDSS155240.40+194816	1.611	46.537	35.068 ± 4.003	46.04	(–, 7202)	sy12	9.647	-0.737	–
38	SDSS083850.15+261105	1.612	47.136	39.073 ± 0.988	46.60	(–, 4038)	sy12	9.42	0.041	–
39	SDSS002948.04-095639	1.616	46.324	66.829 ± 17.563	46.02	(–, 3171)	sy12	8.923	-0.035	–
40	SDSS135023.68+265243	1.617	46.677	44.182 ± 2.062	46.22	(–, 3813)	sy12	9.182	-0.097	–
41	SDSS205554.08+004311	1.618	46.143	57.207 ± 14.318	45.45	(–, 4589)	sy12	8.957	-0.643	–
42	SDSS111949.30+233249	1.62	46.21	67.852 ± 6.652	46.07	(–, 6416)	sy12	9.558	-0.625	–
43	SDSS004149.64-094705	1.622	46.843	35.272 ± 1.085	46.19	(–, 6552)	sy12	9.636	-0.583	–
44	SDSS160456.14-001907	1.629	46.715	42.693 ± 3.359	46.23	(–, 5064)	sy12	9.435	-0.337	1843.61
45	SDSS141949.39+060654	1.638	46.666	28.927 ± 2.503	45.94	(–, 5252)	sy12	9.319	-0.516	–
46	SDSS100401.27+423123	1.653	47.003	20.783 ± 1.471	46.34	(–, 3977)	sy12	9.28	-0.072	–
47	SDSS142841.97+592552	1.653	46.482	35.699 ± 2.802	46.09	(–, 4095)	sy12	9.179	-0.224	–
48	SDSS020044.50+122319	1.656	46.607	28.453 ± 1.061	45.99	(–, 4759)	sy12	9.26	-0.404	–
49	SDSS204536.56-010147	1.658	47.112	37.154 ± 1.789	46.52	(–, 6458)	sy12	9.789	-0.405	–
50	SDSS110240.16+394730	1.659	46.397	34.553 ± 4.662	45.95	(–, 5289)	sy12	9.333	-0.514	–
51	SDSSJ094533.98+10095	1.662	46.46	$2.9^{+0.3}_{-0.6}$	46.17	(–, 4278)	S15	9.257	-0.221	–
52	SDSS094913.05+175155	1.666	46.668	36.279 ± 2.006	46.18	(–, 5581)	sy12	9.493	-0.447	–
53	SDSS213748.44+001220	1.668	46.535	8.204 ± 1.359	45.82	(–, 4163)	sy12	9.056	-0.375	192.41
54	SDSS153859.45+053705	1.681	46.508	34.223 ± 1.528	46.06	(–, 3414)	sy12	9.004	-0.083	–
55	SDSS162103.98+002905	1.681	46.271	28.291 ± 2.598	46.02	(–, 5835)	sy12	9.452	-0.566	–
56	SDSS041255.16-061210	1.684	46.763	32.237 ± 2.201	46.05	(–, 4566)	sy12	9.256	-0.336	–
57	SDSS0246-0825	1.686	46.098	87.842 ± 5.921	44.59	(–, 2500)	A11	8.001	-0.545	–
58	SDSS105951.05+090905	1.688	46.797	84.549 ± 3.086	46.33	(–, 4605)	sy12	9.402	-0.205	–
59	SDSS112542.29+000101	1.689	46.495	84.899 ± 2.669	46.23	(–, 4321)	sy12	9.298	-0.198	79.93
60	SDSS101504.75+123022	1.69	46.632	24.331 ± 1.592	46.11	(–, 4654)	sy12	9.298	-0.327	–
61	SDSSJ141730.92+07332	1.704	46.304	$2.5^{+2.1}_{-0.7}$	45.91	(–, 2784)	S15	8.754	0.022	–

Table 2. – continue

N	Name	z	L_{1350} (erg s^{-1})	EW(C IV) (Å)	L_{5100} (erg s^{-1})	FWHM($H\alpha, H\beta$) (km s^{-1})	ref.	$M_{\rm BH}$ ($M_{\odot}$)	L_{Bol}/L_{Edd}	R
(1)	(2)	(3)	(4)	(5)	(6)	(7)	(8)	(9)	(10)	(11)
62	PG1115+080	1.735	47.303	41.557 ± 0.743	44.93	(–, 4400)	A11	8.662	-0.866	–
63	SDSSJ083650.86+14253	1.745	46.112	$4.2^{+0.3}_{-0.5}$	45.93	(–, 2880)	S15	8.794	0.002	–
64	SDSSJ141141.96+14023	1.745	46.238	$3.8^{+0.8}_{-0.2}$	45.64	(–, 3966)	S15	8.927	-0.420	–
65	SDSS122039.45+000427	2.047	46.838	45.22 ± 1.656	46.39	(–, 3651)	sy12	9.23	0.027	–
66	SDSS143645.80+633637	2.068	47.003	49.388 ± 1.512	46.72	(–, 7056)	sy12	9.969	-0.379	1670.64
67	SDSS014944.43+150106	2.071	46.872	49.012 ± 0.945	46.39	(–, 5969)	sy12	9.657	-0.401	–
68	SDSS143148.09+053558	2.097	47.092	46.011 ± 1.013	46.81	(–, 1327)	sy12	10.561	-0.885	–
69	SDSS142108.71+224117	2.185	47.07	58.384 ± 1.033	46.81	(–, 5964)	sy12	9.868	-0.188	–
70	SDSSJ152156.48+52023	2.208	47.609	9.1 ± 0.6	47.14	(–, 5750)	S15	9.999	0.007	–
71	UM645	2.267	46.696	$39.6^{+9.3}_{-6.0}$	46.31	(–, 3966)	S04	9.262	-0.085	761.41
72	SDSSJ170102.18+61230	2.287	46.632	$18.7^{+3.8}_{-3.2}$	46.34	(–, 5760)	S04	9.601	-0.395	–
73	SDSSJ144245.66-02425	2.325	46.071	$53.7^{+3.0}_{-3.3}$	46.03	(–, 3661)	N07	9.052	-0.156	–
74	SDSSJ115111.20+03404	2.337	45.359	$47.2^{+2.3}_{-2.1}$	45.58	(–, 5146)	N07	9.123	-0.677	–
75	SDSSJ100710.70+04211	2.364	45.898	$55^{+16.0}_{-12.5}$	45.17	(–, 5516)	N07	8.978	-0.942	–
76	UM642	2.371	46.9	$27.8^{+2.3}_{-2.0}$	46.29	(–, 3925)	S04	9.243	-0.086	–
77	SDSSJ125034.41-01051	2.398	45.895	72.3 ± 0.2	45.41	(–, 5149)	N07	9.038	-0.762	–
78	SDSSJ095141.33+01325	2.428	45.699	$87.8^{+5.9}_{-5.3}$	45.55	(–, 4297)	N07	8.951	-0.535	–
79	SDSSJ101257.52+02593	2.433	46.094	$34.9^{+0.6}_{-0.1}$	45.73	(–, 3892)	N07	8.955	-0.359	–
80	SDSS1138+0314	2.443	46.286	79.44 ± 5.242	44.81	(–, 3930)	A11	8.504	-0.828	–
81	UM629	2.462	46.827	$36^{+3.6}_{-3.2}$	46.56	(–, 2621)	S04	9.027	0.399	–
82	SDSSJ025438.37+00213	2.463	46.061	$66.6^{+4.1}_{-2.6}$	45.85	(–, 4164)	N07	9.074	-0.358	–
83	SDSSJ024933.42-08345	2.491	46.655	51.4 ± 0.2	46.38	(–, 5230)	S04	9.537	-0.291	–
84	UM632	2.499	46.851	34.431 ± 3.449	46.54	(–, 3828)	S04	9.346	0.060	1503.53
85	SDSSJ135445.66+00205	2.504	46.79	$21.1^{+2.0}_{-1.7}$	46.49	(–, 2627)	S04	8.994	0.362	–
86	H1413+117	2.56	47.286	35.636 ± 1.393	45.63	(–, 6700)	A11	9.377	-0.881	–
87	Q0142-100	2.73	47.445	31.091 ± 1.087	46.27	(–, 2700)	A11	8.908	0.229	–
88	SDSSJ100428.43+00182	3.045	46.781	$45.4^{+2.9}_{-2.7}$	46.44	(–, 3442)	S04	9.204	0.103	–
89	SBS1425+606	3.192	47.697	$44.7^{+3.2}_{-6.2}$	47.38	(–, 3144)	S04	9.595	0.651	–
90	SDSSJ083700.82+35055	3.311	46.86	53.733 ± 3.084	46.62	(6420, 8162)	J15	9.835	-0.349	–
91	SDSSJ210311.69-06005	3.336	46.473	91.644 ± 5.953	46.30	(–, 6075)	N07	9.627	-0.461	–
92	SDSSJ113838.26-02060	3.343	46.386	$26.1^{+14.4}_{-5.0}$	45.79	(–, 4562)	N07	9.123	-0.467	–
93	SDSSJ210258.21+00202	3.345	46.125	$42.6^{+7.9}_{-6.4}$	45.79	(–, 7198)	N07	9.519	-0.863	–
94	SDSSJ105511.99+02075	3.384	46.374	$49.9^{+11.7}_{-9.3}$	45.70	(–, 5424)	N07	9.229	-0.662	–
95	SDSSJ083630.55+06204	3.4	46.294	$14.9^{+29.7}_{-6.4}$	45.53	(–, 3950)	N07	8.868	-0.472	–
96	SDSSJ123743.08+63014	3.425	46.622	7.7 ± 1.1	46.35	(–, 5200)	S15	9.517	-0.301	–
97	SDSSJ173352.22+54003	3.425	47.418	$22.1^{+16.0}_{-9.6}$	47.00	(–, 3078)	S04	9.387	0.480	13.9
98	SDSSJ115304.62+03595	3.432	46.531	$12.8^{+6.7}_{-3.6}$	46.04	(–, 5521)	N07	9.414	-0.508	–
99	SDSSJ115935.64+04242	3.448	46.599	$45.3^{+4.9}_{-4.6}$	45.92	(–, 5557)	N07	9.36	-0.573	–
100	SDSSJ153725.36-01465	3.452	46.484	$34.5^{+1.5}_{-1.4}$	45.98	(–, 3656)	N07	9.026	-0.18	–
101	SDSSJ114153.34+02192	3.48	46.845	0.4 ± 0.2	46.55	(–, 5900)	S15	9.727	-0.31	11.8
102	SDSSJ164248.71+24030	3.48	46.933	31.321 ± 3.644	46.41	(2500, 3001)	J15	8.911	0.365	–
103	SDSSJ150620.48+46064	3.504	46.893	25.047 ± 2.621	46.38	(6980, 8919)	J15	9.788	-0.541	–
104	SDSSJ142243.02+44172	3.545	47.007	20.796 ± 1.113	47.18	(6110, 7744)	J15	10.072	-0.026	–
105	SDSSJ120934.54+55374	3.573	47.13	7.802 ± 1.401	46.96	(2500, 3001)	J15	9.186	0.64	–
106	SDSSJ075303.33+42313	3.59	47.125	30.149 ± 1.053	46.79	(6240, 7919)	J15	9.895	-0.239	2645.33
107	SDSSJ120447.15+33093	3.616	46.37	126.312 ± 4.401	46.97	(7820,10062)	J15	10.181	-0.345	–
108	SDSSJ101336.37+56153	3.633	46.912	23.303 ± 2.299	46.99	(6650, 8473)	J15	10.051	-0.194	–
109	SDSSJ144144.76+47200	3.633	46.779	63.594 ± 10.716	46.56	(2840, 3435)	J15	9.097	0.33	–
110	SDSSJ145408.95+51144	3.644	47.206	38.895 ± 2.494	47.08	(4680, 5836)	J15	9.79	0.156	–
111	SDSSJ130348.94+00201	3.647	46.736	6.449 ± 1.788	46.73	(6980, 8919)	J15	9.963	-0.366	–
112	SDSSJ015048.83+00412	3.702	46.885	27.598 ± 6.089	46.64	(6470, 8229)	J15	9.852	-0.346	–
113	SDSSJ014049.18-08394	3.713	47.263	24.952 ± 1.253	46.96	(5050, 6327)	J15	9.797	0.030	–
114	SDSSJ113307.63+52283	3.736	46.686	20.66 ± 4.287	46.64	(2500, 3001)	J15	9.026	0.480	–
115	SDSSJ162520.31+22583	3.768	47.136	28.909 ± 1.413	46.66	(5370, 6753)	J15	9.7	-0.174	–
116	SDSSJ012403.77+00443	3.834	47.123	39.35 ± 2.64	46.83	(3760, 4627)	J15	9.475	0.221	–
117	SDSSJ144542.75+49024	3.875	47.288	56.39 ± 3.353	47.12	(6570, 8364)	J15	10.105	-0.119	11.36
118	SDSSJ093554.45+52561	4.005	46.871	26.945 ± 1.766	46.78	(3040, 3693)	J15	9.266	0.380	–
119	SDSSJ132420.83+42255	4.035	46.711	76.709 ± 7.268	46.65	(3330, 4067)	J15	9.28	0.236	–
120	SDSSJ105756.28+45555	4.138	47.343	26.743 ± 1.368	47.24	(4220, 5229)	J15	9.781	0.326	–
121	SDSSJ095511.32+59403	4.336	47.026	46.83 ± 5.299	46.81	(3710, 4561)	J15	9.454	0.222	–
122	SDSSJ083946.22+51120	4.39	46.952	17.834 ± 7.83	46.71	(6220, 7892)	J15	9.853	-0.276	285.1
123	SDSSJ010619.24+00482	4.449	47.002	59.795 ± 5.143	46.80	(7750, 9967)	J15	10.089	-0.422	–
124	SDSSJ134743.29+49562	4.51	47.367	28.466 ± 2.909	46.97	(6780, 8648)	J15	10.057	-0.221	–
125	SDSSJ163636.92+31571	4.559	47.029	12.52 ± 5.536	46.55	(6660, 8486)	J15	9.832	-0.416	–
126	SDSSJ143835.95+43145	4.611	47.422	20.563 ± 2.513	47.14	(4920, 6154)	J15	9.864	0.142	–

Table 3. Summary of the Spearman correlation coefficients and BCES Bisector fit results between C IV EW and $L_{\rm Bol}/L_{\rm Edd}$ for low-z PG QSOs and all QSOs. Col.1: sample; Col.2: QSOs number; Col.3-4: the Spearman-rank correlation coefficient and the probability of the null hypothesis; Col. 5-6: the intercept and the slope from BCES Bisector best-fitting relation, the value in brackets is error.

$Sample$	N	r_s	p	a	b
(1)	(2)	(3)	(4)	(5)	(6)
$low-$z	61	-0.57	2.71×10^{-8}	$1.28(0.08)$	$-0.53(0.10)$
all	160	-0.45	1.52×10^{-11}	$1.35(0.05)$	$-0.58(0.09)$